

Elastic-electron-scattering effects on angular distributions in x-ray-photoelectron spectroscopy

A. Jablonski

Institute of Physical Chemistry, Polish Academy of Sciences, ulica Kasprzaka 44/52, 01-224 Warszawa, Poland

C. J. Powell

Surface and Microanalysis Science Division, National Institute of Standards and Technology, Gaithersburg, Maryland 20899

(Received 9 March 1994)

Electron trajectories in x-ray photoemission from solids are partially randomized by elastic collisions, and thus the angular distribution of photoelectrons leaving the surface is different from that for isolated atoms. This problem is approached in the present work by extensive Monte Carlo simulations of electron trajectories resulting from photoionization of the gold $4s$, $4p_{3/2}$, $4d_{5/2}$, and $4f_{7/2}$ subshells by Mg characteristic x rays. Calculations were made for the full range of angles of x-ray incidence and for all possible positions of the electron energy analyzer. In comparisons with intensities predicted from the common formalism in which elastic scattering is neglected, it was found that the elastic-scattering effects can be accounted for with two correction factors. These factors are, to a large extent, independent of experimental geometry for certain ranges of angles. The correction factors depend only slightly, for example, on the photoelectron exit angle in the range 0° – 30° with respect to the surface normal. The present results indicate that the magic angle (the angle between the direction of x rays and the direction of signal electrons at which the effects of angular anisotropy can be avoided) is not a single constant value of 54.7° (as found for isolated atoms) but a much larger value that depends on the electron exit angle and the photoelectron subshell. Furthermore, it has been found that elastic-scattering effects can be neglected for certain experimental configurations. The current for a given photoelectron line is then equal to the current calculated from the common formalism, but this equality occurs at different angles between the incident x rays and the detected electrons depending on the photoelectron line and the electron exit angle.

I. INTRODUCTION

Much attention has been devoted recently to the problem of elastic scattering of photoelectrons in x-ray-photoelectron spectroscopy (XPS).^{1–10} In most published studies, this problem has been approached theoretically by the use of Monte Carlo algorithms that simulate the photoelectron trajectories in solids. The Monte Carlo (and other) analyses have demonstrated that elastic scattering significantly modifies the distribution of trajectories for the signal photoelectrons and needs to be considered in quantitative XPS analyses. The importance of elastic-scattering effects in XPS has also been demonstrated experimentally.^{2,8}

Careful analysis of the results of Monte Carlo calculations has shown that only a relatively simple correction of the simple formalism commonly used for XPS analyses is necessary to predict the correct photoelectron current from a homogeneous specimen that is recorded by the analyzer.^{3,8,9} It is sufficient to replace the atomic photoelectric cross section

$$d\sigma_x/d\Omega = \sigma_x W(\psi, \beta) = \sigma_x \frac{1}{4\pi} \left[1 - \frac{\beta}{4} (3 \cos^2 \psi - 1) \right] \quad (1)$$

by the cross section modified as follows:^{3,8,9}

$$(d\sigma_x/d\Omega)_{el} = \sigma_x Q_x W(\psi, \beta_{eff}) \\ = \sigma_x Q_x \frac{1}{4\pi} \left[1 - \frac{\beta_{eff}}{4} (3 \cos^2 \psi - 1) \right]. \quad (2)$$

In the above expressions, σ_x denotes the total photoelectric cross section for a particular atom, ψ is the angle between the direction of electron analysis and the direction of x rays, β is the asymmetry parameter, β_{eff} is the effective asymmetry parameter describing the actual angular anisotropy of the measured photoelectron signal, and Q_x is a parameter describing the decrease of intensity due to elastic collisions. The last two parameters can be derived from the results of Monte Carlo calculations that provide realistic simulations of photoelectron trajectories in a solid. The two parameters can be considered as correction factors that account for elastic-scattering effects. It is also important to note that the above formalism is based on the use of unpolarized radiation (the most common practical application).

Equation (2) has been derived from Monte Carlo simulations made from a limited number of experimental geometries: (i) direction of analysis normal to the sample surface and a varying angle of incident x ray,^{3,9} and (ii) direction of x rays normal to the surface and a varying angle of analysis.⁸ The validity of this equation will be analyzed further in the present work by extensive Monte Carlo simulations of photoelectron transport in gold for all possible combinations of the angle of analysis and the

direction of x rays. Gold has been selected for analysis because the elastic-scattering effects are pronounced for elements of high atomic number. Furthermore, the theory of photoelectron transport compares well with experimental data on the angular XPS signal distribution collected for this element.⁸

II. THEORY

Here we outline briefly the common formalism of XPS. The differential photoelectron current entering the analyzer and arising from an infinitesimally thin layer of a homogeneous solid at a depth z is described by the expression

$$dI^{\text{nel}} = I_0 \Delta\Omega (d\sigma_x/d\Omega) AN \exp[-z/(\lambda \cos\alpha)] dz, \quad (3)$$

where I_0 is the flux of incident x rays, $\Delta\Omega$ is the acceptance solid angle of the analyzer, A is the area analyzed (as viewed by the analyzer), N is the atomic density (number of analyzed atoms per unit volume), λ is the inelastic mean free path, and α is the angle of analysis with respect to the surface normal. The superscript "nel" indicates that elastic collisions of the photoelectrons are neglected within the above formalism. The analysis area is usually assumed to depend on the angle α according to

$$A = A_0 / \cos\alpha,$$

where A_0 is the area analyzed at $\alpha=0$. On integration of Eq. (3), we obtain the well-known expression

$$I^{\text{nel}} = I_0 \Delta\Omega (d\sigma_x/d\Omega) A_0 N \lambda. \quad (4)$$

The results of a more realistic theoretical model that takes elastic collisions of the photoelectrons into account cannot be expressed by a simple analytical formula. It is convenient to use the Monte Carlo algorithm for simulating elastic and inelastic collisions of the photoelectrons in a solid. For the sake of brevity, the interested reader is referred to the literature for details on calculations of the elastic-scattering cross sections^{11,12} and the Monte Carlo scheme.⁸ In the present work, only a brief outline of the algorithm is given below.

The following assumptions are made here.

(1) The interaction between a photoelectron and the scattering center is described by the Thomas-Fermi-Dirac potential.¹³

(2) The elastic-scattering cross sections are calculated from the relativistic partial-wave expansion method (PWEM).

(3) Photoelectrons are created with a uniform distribution with respect to depth. This assumption is reasonable in view of the considerably larger penetration depth of x rays as compared to the sampling depth for the signal photoelectrons in XPS.

(4) The solid is assumed to be amorphous or polycrystalline. Thus diffraction effects are neglected.

At first, a photoelectron is emitted according to the angular distribution associated with the photoelectric cross section

$$G(\theta_e) = [2\pi(d\sigma_x/d\Omega)\sin\theta_e] / \sigma_x,$$

where θ_e is the ejection angle with respect to the surface normal. The photoelectron trajectory is then followed until either the photoelectron leaves the solid or until the total trajectory length becomes excessively large (and thus the probability of no inelastic scattering becomes negligibly small). Along the trajectory, the photoelectron undergoes elastic collisions, and the corresponding scattering angles ω follow a distribution based on the differential elastic-scattering cross section $d\sigma/d\Omega$:

$$H(\omega) = [2\pi(d\sigma/d\Omega)\sin\omega] / \sigma_t,$$

where σ_t is the total elastic-scattering cross section. The photoelectron current collected by the analyzer is calculated from

$$I^{\text{el}} = \lim_{n \rightarrow \infty} \frac{1}{n} \sum_{i=1}^n \Delta I_i,$$

where n is the number of trajectories, ΔI_i is the contribution to the photoelectron current associated with the i th trajectory, and the superscript "el" indicates that elastic collisions have been taken into account. The current ΔI_i is calculated according to the following rule:

$$\Delta I_i = \begin{cases} \exp(-x_i/\lambda) & \text{if the electron leaves the} \\ & \text{solid within the solid} \\ & \text{angle of the analyzer} \\ 0 & \text{in all other cases,} \end{cases}$$

where x_i is the total trajectory length in the solid. Thus the Monte Carlo algorithm requires knowledge of the inelastic mean free path and the asymmetry parameter for a given photoelectron. In the present work, values of λ were taken from Tanuma, Powell, and Penn,¹⁴ and values of β from Band, Kharitonov, and Trzhaskovskaya.¹⁵

As mentioned above, the results of Monte Carlo calculations are well approximated by Eq. (4) with the modified photoelectric cross section given by Eq. (2). We can then write the total current of signal photoelectrons:

$$I^{\text{el}} = I_0 \Delta\Omega (d\sigma_x/d\Omega)_{\text{el}} A_0 N \lambda \\ = I_0 \Delta\Omega A_0 N \lambda \sigma_x Q_x W(\psi, \beta_{\text{eff}}). \quad (5)$$

The correction factors Q_x and β_{eff} have been reported in the literature for selected photoelectron lines and experimental geometries.^{3,8} In the present work, we examine fits of the approximate equation (5) to the results of the Monte Carlo calculations for XPS from gold in all possible geometries.

III. RESULTS

Figure 1 shows a schematic outline for the XPS configuration. The direction of the incident x rays, θ , the average electron detection angle α , and the surface normal are assumed to be in one plane. The photoelectron intensities I^{el} are calculated from selected fixed detection angles α and for selected x-ray incidence angles θ . The angle θ is assumed to be positive if the x-ray source and analyzer are located on different sides of the surface normal (as in Fig. 1), or negative if the x-ray source is on the

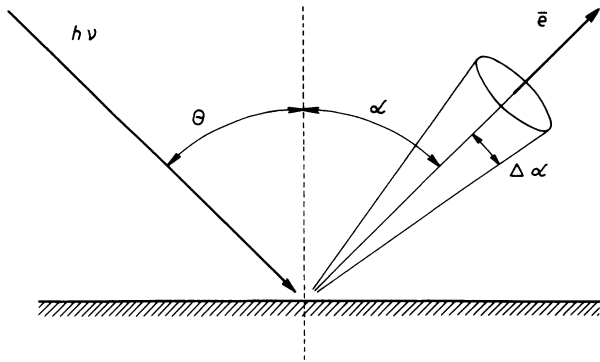


FIG. 1. Schematic outline of the XPS configuration for the calculations. The angle θ is negative if the direction of the x rays and the analyzer axis are on the same side of the surface normal.

same side as the analyzer. The size of the half-cone angle $\Delta\alpha$ of the analyzer determines the number of trajectories necessary to reach reasonable precision. This solid angle cannot be too small since the probability that a photoelectron enters the analyzer becomes very small, and then the number of generated trajectories has to be increased considerably. On the other hand, the angle $\Delta\alpha$ cannot be too large because the simulations would not then be realistic for practical analyzers (for which $\Delta\alpha$ typically ranges from 2° to 7°). The value of $\Delta\alpha = 10^\circ$ was found to be a good compromise; this value gives a precision of $\pm 2\%$ (standard deviation) after the generation of 2×10^6 trajectories. Monte Carlo simulations were made for different detection angles ranging from 0° to 80° (in 10° steps), and for angles of x-ray incidence ranging from -85° to $+85^\circ$ (in 5° steps).

Calculations were performed for photoelectrons ejected by Mg $K\alpha$ radiation from gold, i.e., for the Au $4s$, Au $4p_{3/2}$, Au $4d_{5/2}$, and Au $4f_{7/2}$ subshells. The results of the calculations are shown in Figs. 2(a)–2(d). In all cases, the calculated intensities (open circles) are well fitted by Eq. (5) (solid lines). Furthermore, comparison with the intensities expected from the common formalism in which elastic scattering is neglected (dotted line) shows significant differences from the more realistic Monte Carlo simulations. The anisotropy in the angular dependence of the photoelectron intensity is always decreased by elastic scattering; that is, the effective asymmetry parameter β_{eff} is less than the asymmetry parameter β for photoemission from the source atom.

The decrease in the angular anisotropy, however, is dependent on the detection angle α . Figures 3(a)–3(d) show the dependence of the correction factors β_{eff} and Q_x on α . For $\alpha < 60^\circ$, the variation of β_{eff} and Q_x with α is rather weak. At larger detection angles, the dependence of both β_{eff} and Q_x on α becomes more pronounced. The dependence of both correction factors on detection angle can be well fitted by the simple polynomials

$$\beta_{\text{eff}} = a_\beta \cos^2 \alpha + b_\beta \cos \alpha + c_\beta, \quad (6a)$$

$$Q_x = a_Q \cos^2 \alpha + b_Q \cos \alpha + c_Q. \quad (6b)$$

The parameters of the polynomial fit for each photoelectron line are listed in Table I. Equations 6(a) and 6(b), together with the modified photoelectric cross section [Eqs. (2) and (5)], provide a complete description of the elastic-scattering effects for *any* experimental geometry with an accuracy comparable to the precision of the Monte Carlo calculations (about 2%).

IV. SPECIAL ANGLES

A. Magic angle

The differential cross section for photoionization from atoms [Eq. (1)] is anisotropic for common XPS conditions. The extent of the anisotropy depends on the value of β which is a function of photon energy, atomic number Z , and the particular subshell.^{15,16} Attention has been drawn to the fact that the photoelectron intensity for a certain angle ψ between the direction of x rays and the direction of analysis will be the same as if the photoemission were assumed to be isotropic; this angle, $\psi = 54.7^\circ$ or $54^\circ 44' 8''$ is frequently referred to as the “magic angle.”^{16–18} To the authors’ knowledge, Huang, Rabalais, and Ellison¹⁷ seem to be the first to have used this term, although Samson¹⁹ indicated the special role of this angle in 1969.

Reilman, Msezane, and Manson¹⁶ suggested that XPS measurements should be made with ψ set to the magic angle in order to avoid the need for a correction due to the angular anisotropy of photoionization. However, we have seen in Sec. III that elastic electron scattering in solids modifies the photoelectron angular distribution, and thus β_{eff} differs from β for the Au subshells. We now investigate the extent to which elastic scattering modifies the magic angle.

We assume for the moment that the photoelectron emission is isotropic, i.e., the asymmetry parameter is equal to zero. If elastic scattering is also neglected, the photoelectron current predicted from Eq. (4) becomes

$$I^{\text{nel, is}} = I_0 \Delta \Omega \sigma_x A_0 N \lambda / 4\pi. \quad (7)$$

At the magic angle ψ_M the signal current expected from the oversimplified Eq. (7) should be identical to the signal current expected from the common formalism (elastic scattering neglected); that is,

$$I^{\text{nel, is}} = I^{\text{nel}}. \quad (8)$$

Equations (4), (7), and (8) give

$$1 = 1 - \beta(3 \cos^2 \psi_M - 1) / 4$$

or

$$\cos \psi_M = (\frac{1}{3})^{1/2}, \quad \psi_M = 54^\circ 44' 8''.$$

The magic angle derived from Eq. (8) thus does not depend on β .^{16–18}

The angular distribution of the photoelectron current is better described by Eq. (5) (elastic scattering included) than by Eq. (4). The magic angle should then be determined from

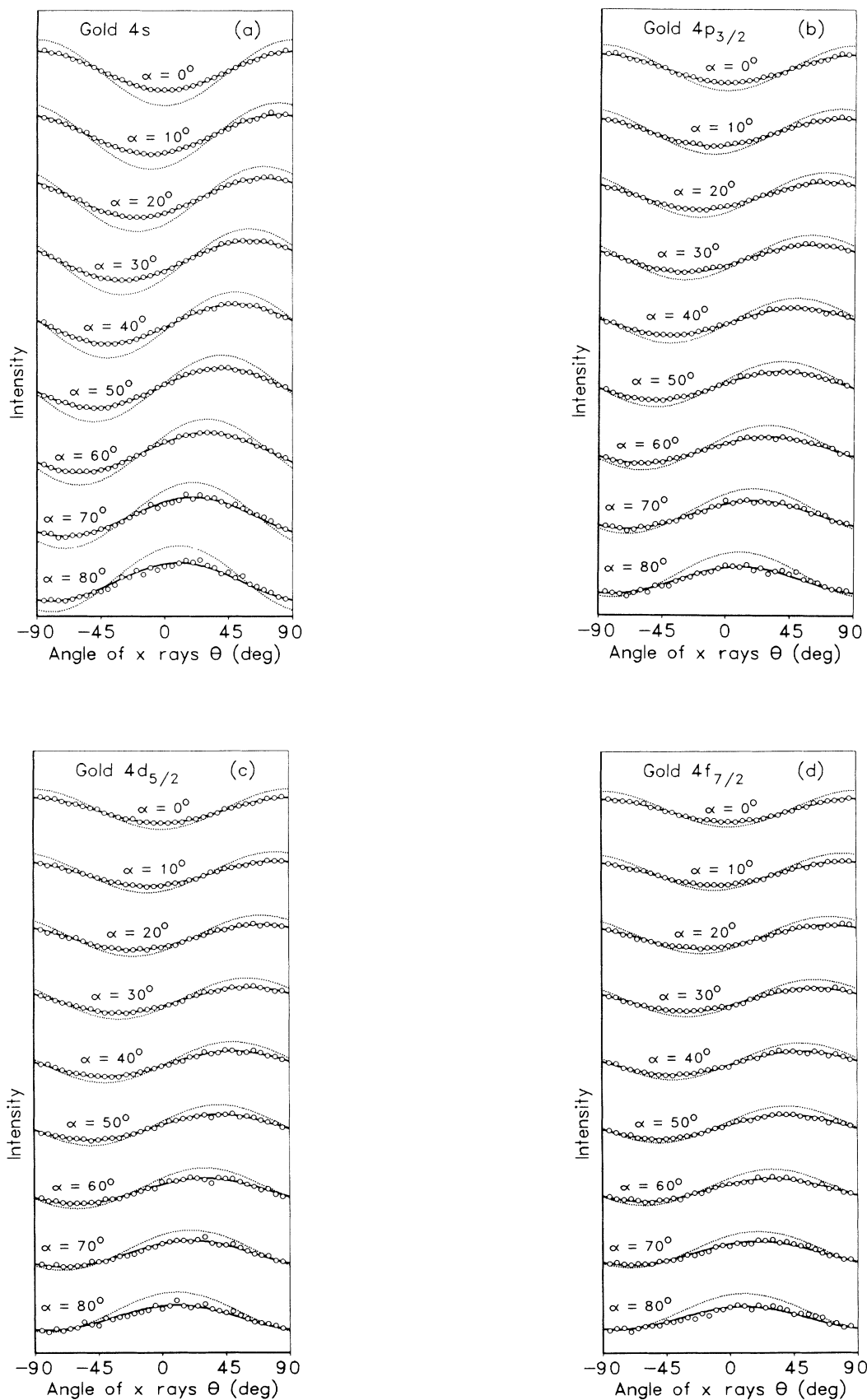


FIG. 2. Dependence of the photoelectron intensity on the detection angle α , and the angle of x rays, θ . Dotted line: common formalism [Eq. (4)]; circles: results of Monte Carlo calculation using a model that accounts for elastic photoelectron collisions; solid line: modified formalism [Eq. (5)]. (a) Au 4s; (b) Au 4p_{3/2}; (c) Au 4d_{5/2}; (d) Au 4f_{7/2}.

$$I^{\text{nel, is}} = I^{\text{el}} \quad (9)$$

rather than from Eq. (8). From Eqs. (5), (7), and (9), we have

$$1 = Q_x \left[1 - \frac{\beta_{\text{eff}}}{4} (3 \cos^2 \psi_M - 1) \right]$$

and

$$\cos \psi_M = \left\{ \frac{1}{3} \left[1 + \frac{4}{\beta_{\text{eff}}} \left(1 - \frac{1}{Q_x} \right) \right] \right\}^{1/2}. \quad (10)$$

Since the correction factors β_{eff} and Q_x are functions of the detection angle α , the angle ψ_M from Eq. (10) will also depend on α . Furthermore, both correction factors depend on the photoelectron line [Figs. 3(a)–3(d)], and thus the dependence of the magic angle on α is expected

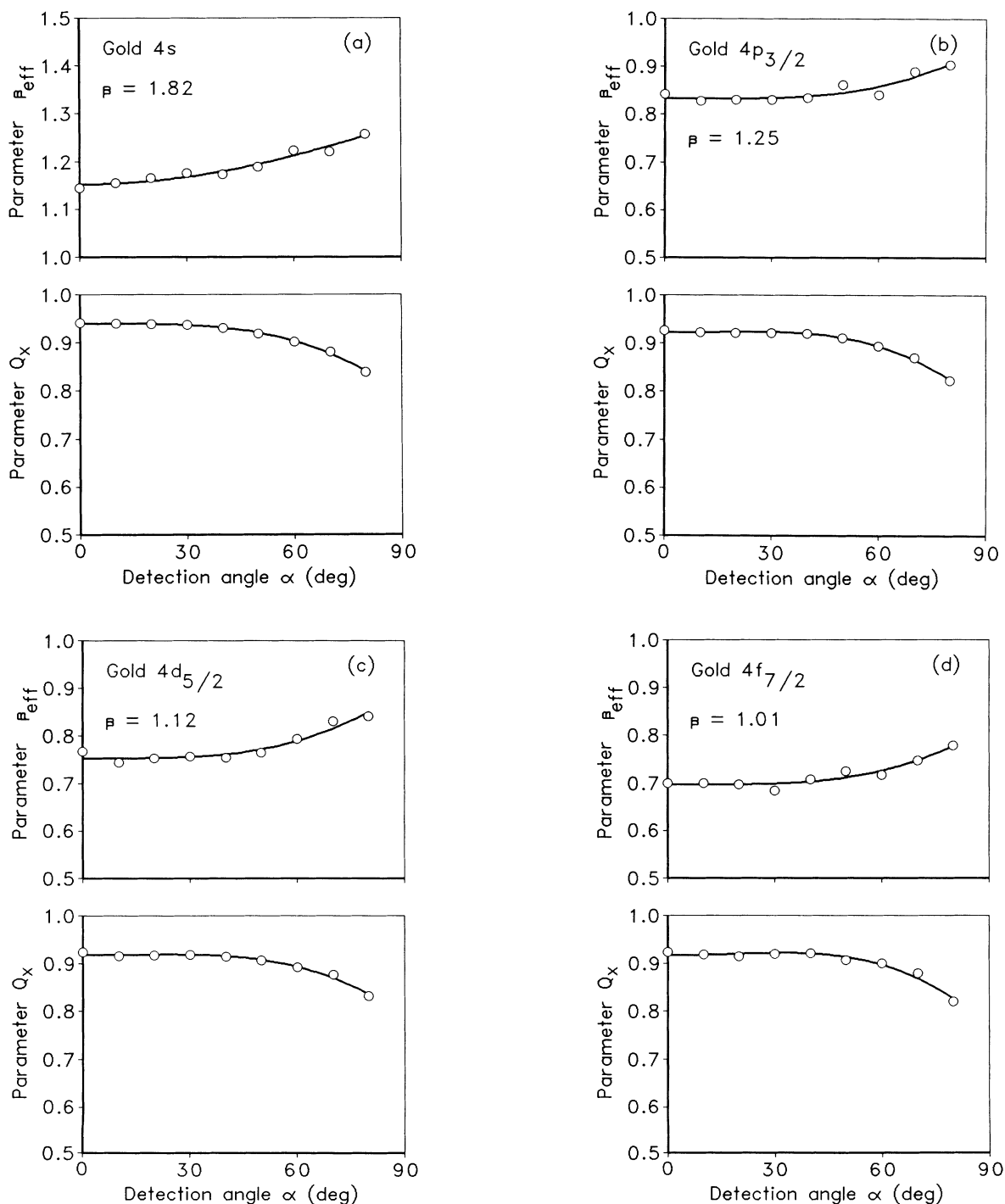


FIG. 3. Dependence of the correction factors β_{eff} and Q_x on the detection angle α . Circles: values derived from Monte Carlo calculations; solid line: fit of Eqs. (6a) and (6b). The value of β given in the upper panel is for the free atom (Ref. 12). (a) Au 4s; (b) Au 4p_{3/2}; (c) Au 4d_{5/2}; (d) Au 4f_{7/2}.

TABLE I. Values of the fitted parameters describing the detection angle dependence of the correction parameters β_{eff} and Q_x [Eqs. (6a) and (6b)].

Fitted parameter	Au 4s	Au 4p _{3/2}	Au 4d _{5/2}	Au 4f _{7/2}
a_β	0.008 387 50	0.116 219	0.137 583	0.121 845
b_β	-0.132 594	-0.225 597	-0.278 803	-0.239 818
c_β	1.276 32	0.942 751	0.894 648	0.814 962
a_Q	-0.141 447	-0.185 611	-0.152 496	-0.214 553
b_Q	0.285 835	0.335 339	0.278 138	0.361 490
c_Q	0.795 438	0.772 480	0.792 530	0.769 893

to be different for the different photoelectron lines. Figure 4 indicates that the dependence of the magic angle on detection angle is rather weak for $\alpha < 30^\circ$ but becomes stronger for larger values of α . We also observe a pronounced dependence of the magic angle on the photoelectron line. Thus, in reality, the magic angle is not a single value common to all photoelectron lines with different β values, but has a range extending from about 60° to 80° .

We now calculate an average magic angle from the data presented in Fig. 4. We limit consideration to the range $0 < \alpha < 45^\circ$, where the variation of the relation ψ_M vs α is the smallest (Fig. 4), and average the functions ψ_M vs α according to the obvious formula

$$\langle \cos \psi_M \rangle = \frac{1}{(1 - \cos 45^\circ)} \frac{1}{4} \sum_{i=1}^4 \int_{\cos 45^\circ}^1 \cos^{(i)} \psi_M d(\cos \alpha), \quad (11)$$

where $\cos^{(i)} \psi_M$ is given by Eq. (10), and the index “ i ” indicates the subshells from which photoelectrons origi-

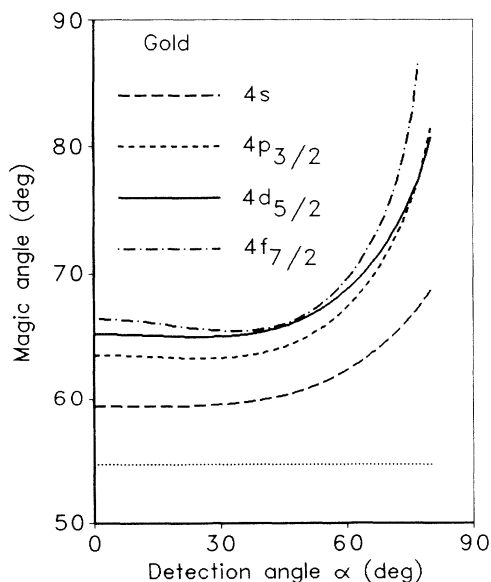


FIG. 4. The dependence of the magic angle derived from Monte Carlo calculations on the detection angle. Long-dashed line: Au 4s; short-dashed line: Au 4p_{3/2}; solid line: Au 4d_{5/2}; dot-dashed line: Au 4f_{7/2}; dotted line: the value of $54^\circ 44' 8''$.

nate. From Eq. (11), we obtain $\langle \cos \psi_M \rangle = 0.445 094$, i.e., $\psi_M^{\text{ave}} = 63^\circ 34'$. This value is considerably larger than the magic angle for isolated atoms (54.7°).

B. Master angle

We see from Figs. 2(a) and 2(b) that the curve for the photoelectron intensity as a function of angle of x-ray incidence from the common formalism (elastic scattering neglected) intersects the photoelectron intensity found from the Monte Carlo calculations for all cases considered here. Thus, for certain experimental geometries, the common formalism gives the correct photoelectron intensity. We then have

$$I^{\text{el}} = I^{\text{nel}}. \quad (12)$$

We define ψ_0 as the angle between the x-ray direction and the analysis direction for which Eq. (12) is satisfied. XPS measurements made with this configuration would then be expected to circumvent the effects of elastic collisions. For brevity, we will refer to ψ_0 as the master angle. From Eqs. (4), (5), and (12), we obtain

$$1 - \frac{\beta}{4} (3 \cos^2 \psi_0 - 1) = Q_x \left[1 - \frac{\beta_{\text{eff}}}{4} (3 \cos^2 \psi_0 - 1) \right]$$

and

$$\cos \psi_0 = \left[\frac{1}{3} \left(1 + \frac{4(1 - Q_x)}{\beta - \beta_{\text{eff}} Q_x} \right) \right]^{1/2}. \quad (13)$$

It is obvious from Eq. (13) that there is no single universal value of the master angle for which the elastic-scattering effects are avoided. As for the magic angle, the angle ψ_0 depends on the angle α and the photoelectron line; Fig. 5 illustrates these dependences. We see also

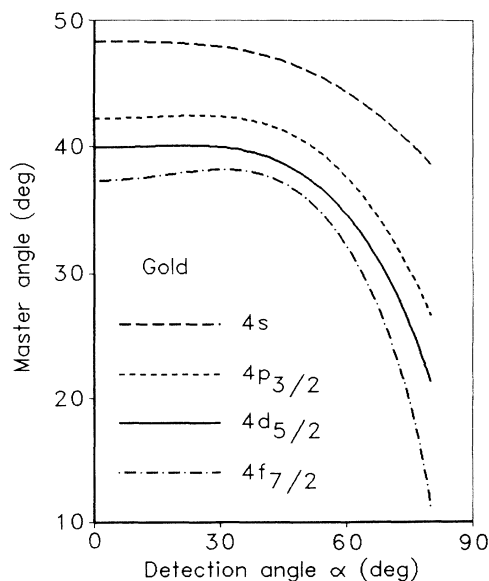


FIG. 5. The dependence of the master angle on the detection angle. Long-dashed line: Au 4s; short-dashed line: Au 4p_{3/2}; solid line: Au 4d_{5/2}; dot-dashed line: Au 4f_{7/2}.

that the dependence of ψ_0 on the detection angle becomes more pronounced for $\alpha > 30^\circ$. Distinctly different functions are observed for the different photoelectron lines. Finally, the master angle, ranging from about 10° to 48° , is always smaller than the corresponding magic angle.

We now calculate an average value of the master angle using the approach we employed for the average magic angle [Eq. (11)]. We again limit consideration to the range $0 < \alpha < 45^\circ$ where the variation of the master angle is small (Fig. 5). We then have

$$\langle \cos \psi_0 \rangle = \frac{1}{(1 - \cos 45^\circ)} \frac{1}{4} \sum_{i=1}^4 \int_{\cos 45^\circ}^1 \cos^{(i)} \psi_0 d(\cos \alpha),$$

where $\cos^{(i)} \psi_0$ is given by Eq. (13), and again the index "i" indicates a particular Au subshell. We obtain $\langle \cos \psi_0 \rangle = 0.743076$ and thus $\psi_0^{\text{ave}} = 42^\circ 1'$.

V. DISCUSSION

The reliability of the results reported in the present paper is directly related to the quality of the theoretical model of electron transport used in the calculations. Similar Monte Carlo calculations have proven to be reliable in other studies. It has been demonstrated experimentally that the angular distributions of photoemission from aluminum^{2,8,20} and gold⁸ surfaces differ significantly from the corresponding distributions for atoms. The measured photoelectron angular distributions for the solids are also well described by a model of photoelectron transport in which elastic collisions are included.^{2,8,20} Finally, similar Monte Carlo simulations of elastic electron backscattering at medium energies compare well with experimental data.^{11,12,21}

The importance of making a correction for the angular anisotropy of photoionization in quantitative XPS has been pointed out previously.^{22,23} The effective asymmetry parameter β_{eff} for photoemission from solid surfaces is found always to be less than the corresponding value of β for atoms on account of elastic scattering in the solid.

It has been suggested¹⁶ that XPS analyses made with an instrument having $\psi = 54.7^\circ$ would be simplified by not having to make the anisotropy correction. This suggestion was made before the effects of elastic electron scattering in XPS were realized. We have shown here that the magic angle depends on the photoelectron line and the detection angle α (Fig. 3); in all instances, the calculated magic angle was greater than 54.7° .

It is of interest to calculate the systematic error due to elastic scattering that would be introduced on an instrument with $\psi = 54.7^\circ$ if the angular-anisotropy correction was ignored. Figure 6 shows one of the sets of data from Fig. 2(a) to illustrate the systematic error of measurements made with $\psi = 54.7^\circ$; for $\alpha = 70^\circ$, $\theta = 55.3^\circ$, and $\theta = -15.3^\circ$ as indicated by the thin vertical lines. The thick vertical lines in Fig. 6 indicate the systematic error for the chosen conditions. We also indicate in Fig. 6 the positions of the master angle by the vertical dashed lines. For the chosen conditions, $\psi_0 = 42.32^\circ$ and corresponding values of θ are -27.68° and 67.68° .

We define the percentage deviation δ by

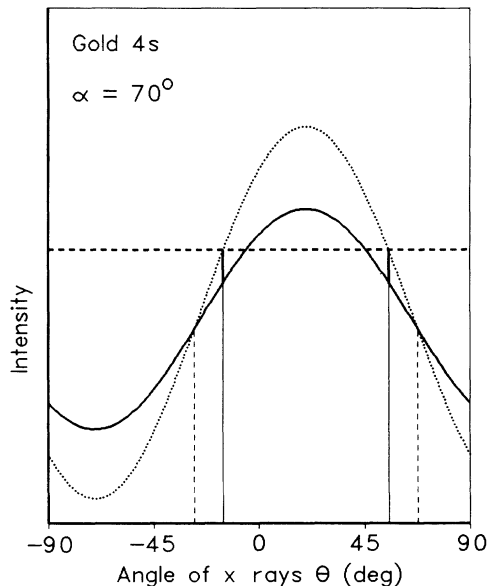


FIG. 6. Dependence of the Au 4s photoelectron intensity recorded at $\alpha = 70^\circ$ on the angle of x rays, θ . Dotted line: common formalism (I^{nel}); solid line: modified formalism accounting for elastic photoelectron collisions (I^{el}); horizontal dashed line: model assuming isotropic photoelectron emission ($I^{\text{nel, is}}$). The vertical solid lines denote values of θ for which $\psi_M = 54.7^\circ$ (the magic angle for free atoms). The heavy vertical lines indicate the difference between $I^{\text{nel, is}}$ and I^{el} that is plotted in relative form [Eq. (14)] in Fig. 7. The vertical dashed lines denote values of θ for which $I^{\text{el}} = I^{\text{nel}}$; for the present conditions, the master angle $\psi_0 = 42.32^\circ$.

$$\delta = 100(I^{\text{nel, is}} - I^{\text{el}})/I^{\text{el}}, \quad (14)$$

where $I^{\text{nel, is}}$ is the photoelectron current if there is no angular anisotropy [Eq. (7)], and I^{el} is the more realistic photoelectron current [Eq. (5)] that includes angular-anisotropy and elastic-scattering effects; for $\psi = 54.7^\circ$, $I^{\text{nel, is}} = I^{\text{nel}}$ [Eq. (4)]. Figure 7 shows a plot of δ versus the detection angle α for $\psi_M = 54.7^\circ$ for the different Au photoelectron lines. We see that δ can exceed 20% for glancing takeoff angles. Figure 8 shows a similar plot of δ vs α , where δ has now been calculated for $\psi_M^{\text{ave}} = 63^\circ 34'$; as expected, the deviations are much less than those in Fig. 7. The magnitude of δ will probably be different for other elements and photoelectron lines, and we conclude that a specific correction for angular anisotropy will probably be necessary even if XPS measurements are made with $\psi = 54.7^\circ$ (or even for another fixed angle such as $63^\circ 34'$).

The deviations of the magic angle values calculated here (Fig. 4) from 54.7° are due to the effects of elastic scattering in solids. It would be reasonable to expect that the magic angle for solids should approach 54.7° as the elastic-scattering effects become weaker, but the present results indicate a more complex behavior. For example, the elastic-scattering effects should decrease with increasing photoelectron energy. However, we see in Fig. 4 that the curve with the smallest deviation from 54.7° is for the 4s photoelectrons which have the lowest energy, while

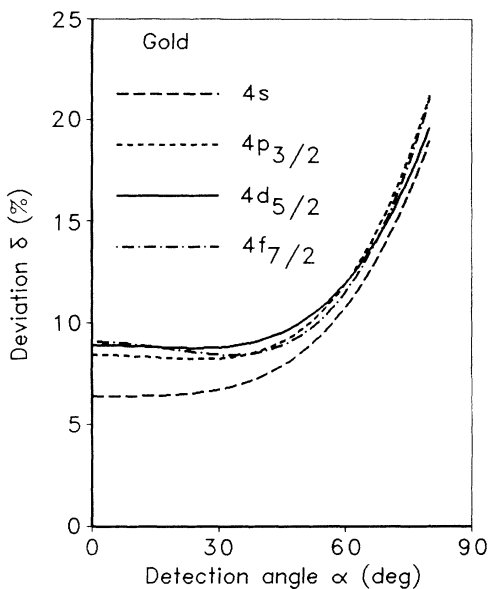


FIG. 7. The percentage deviation between photoelectron intensities calculated from Eq. (14) for $\psi_M = 54.7^\circ$. Long-dashed line: Au 4s; short-dashed line: Au 4p_{3/2}; solid line: Au 4d_{5/2}; dot-dashed line: Au 4f_{7/2}.

the deviation of the other curves from 54.7° generally increases with increasing kinetic energy. There are two reasons for this result.

(a) The parameter Q_x describing the decrease in the photoelectron current due to elastic scattering is practically identical for the four photoelectron lines considered here [Figs. 3(a)–3(d)].

(b) The value of the effective angular anisotropy for the four photoelectron lines decreases strongly in the order Au 4s > Au 4p_{3/2} > Au 4d_{5/2} > Au 4f_{7/2}, i.e., in the or-

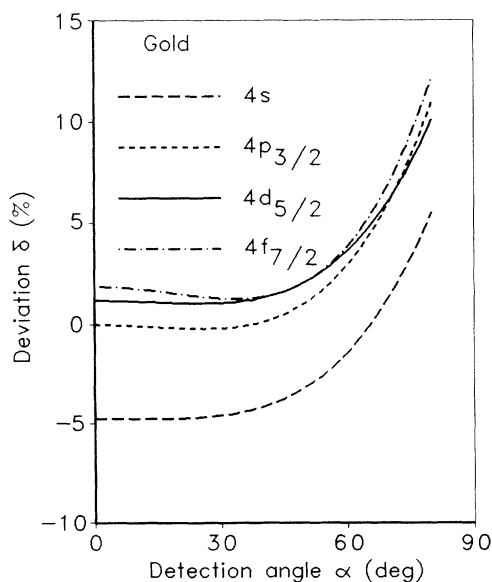


FIG. 8. The percentage deviation between photoelectron intensities calculated from Eq. (14) as in Fig. 7, but for $\psi_M^{ave} = 63.34^\circ$.

der of increasing kinetic energy. In effect, the multiplication of $W(\psi, \beta_{eff})$ by Q_x [Eq. (2)] is stronger for lines with small anisotropy, i.e., larger kinetic energy. This conclusion can also be deduced from Fig. 6. For small values of β (and simultaneously small values of β_{eff}), the solid line may become nearly tangent to the dashed line ($I^{nel, is}$), and the point of intersection may then deviate considerably from the atomic value for the magic angle (54.7°). At still smaller values of β , the curves may not even intersect. We conclude that the deviations of the magic angles in solids from 54.7° is due largely to the angular anisotropy in the photoelectron emission. Another option in instrumental design is to set ψ equal to the master angle ψ_0 [Eq. (13)]. We see from Fig. 5 that the average value of ψ_0 for the four Au photoelectron lines is about 42° if $\alpha < 45^\circ$. For such a configuration, only a small correction for elastic scattering would be required; a correction would also then be needed for the angular anisotropy. Similar calculations for other elements will indicate the extent to which the master angle is a function of atomic number.

Knowledge of the angular distribution of photoemission from solids is of importance in some procedures of quantitative analysis by XPS. An example is the method proposed by Ebel, Ebel, and Hirokawa²⁴ and Hanke *et al.*,²⁵ in which the sensitivity factor S relating the signal strength to the concentration is expressed within the common formalism [Eqs. (1) and (4)] by the following function:

$$S = CT(E)(d\sigma_x/d\Omega)\lambda, \quad (15)$$

where C is a constant that depends on the specimen material and the set of instrumental conditions, and $T(E)$ is the spectrometer function. The method of Ebel, Ebel, and Hirokawa²⁴ and Hanke *et al.*²⁵ consists of calculating the sensitivity factor for each line from Eq. (15) and then determining the surface composition from the measured photoelectron signal intensities. The photoelectric cross section should actually be calculated from Eq. (2). We conclude that the use of Eq. (1), for which elastic-scattering effects are neglected, may lead to systematic errors in quantitative XPS analyses by the method of Ebel, Ebel, and Hirokawa.

Another situation in which elastic-scattering effects are expected to be important is in the use of angle-resolved XPS (ARXPS) to determine composition profiles in near-surface regions.²⁶ Changes in the anisotropy of photoemission due to elastic photoelectron collisions are neglected in the current formalism of ARXPS.²⁶ Werner, Smith, and Livesy²⁷ have recently shown that the neglect of elastic photoelectron collisions considerably influences the recovered composition profile. The composition-depth profiles may therefore be subject to additional error, particularly since it is known that the deduced profiles are often sensitive to small errors in measured intensities or intensity ratios. The simple parametrization of the elastic-scattering effects proposed here [Eq. (6)] may be useful in making corrections to the ARXPS formalism. For this purpose, however, extensive information would be needed about the correction pa-

parameters β_{eff} and Q_x and their dependence on material composition.

Unfortunately, there are only a limited number of values for the correction factors β_{eff} and Q_x now available in the literature. It would be useful to create a database of the correction factors for all significant photoelectron lines and for the commonly used radiations. For this purpose, it should be sufficient to list the six fitted parameters for each line [Eqs. 6(a) and 6(b)] to obtain correction factors valid for all experimental geometries. Such calculations are planned.

The calculations reported here require considerable computational effort. This situation is due to the fact that the analyzer has a relatively small solid angle. Consequently, a large number of photoelectron trajectories must be generated to estimate intensities with reasonable precision. One may think that a different Monte Carlo scheme could be used in which the problem of having a small solid analyzer angle is not crucial, i.e., the trajectory reversal approach.^{5,6,28} This approach is well suited for calculating the so-called depth distribution function, i.e., the function describing contributions to the recorded signal arising from different depths. Due to problems with normalization of the results, the trajectory reversal method does not seem applicable, at least presently, for calculating the photoelectron intensities.

VI. SUMMARY

We have investigated the effects of elastic electron scattering on the angular distributions of photoelectrons in an XPS experiment for a wide range of possible configurations. An extensive series of Monte Carlo calculations has been performed to simulate photoemission from the 4s, 4p_{3/2}, 4d_{5/2}, and 4f_{7/2} subshells of gold by Mg characteristic x rays. These simulations were made for angles of x-ray incidence ranging from -85° to 85° with respect to the surface normal, for average electron

exit angles varying from 0° to 80°, and for an assumed analyzer half-cone angle of 10°. The simulations were performed for gold to illustrate the effects of relatively strong elastic scattering in elements of high atomic number.

Photoelectron intensities from the Monte Carlo simulations were compared with those expected from the common XPS formalism, in which elastic scattering is neglected. It was found earlier that the effects of elastic scattering can be accounted for by the inclusion of two correction factors in the common formalism. One of these factors accounts for a reduction in XPS intensity, and the other is an effective angular asymmetry parameter which is appreciably less than the corresponding value for free atoms. The present work has shown that these two correction factors provide reliable corrections for elastic scattering over a much wider range of possible experimental configurations than had been investigated previously. The correction factors do not change significantly with electron exit angle in the range 0–30°.

It is known that the effects of angular anisotropy in XPS from free atoms or molecules can be avoided by making measurements when the angle ψ between the direction of the x ray and the direction of signal electrons is set to 54.7° (the magic angle). In XPS from solid gold, however, the magic angle is larger than 54.7° and depends on the electron exit angle and the photoelectron subshell. It was also found that the photoelectron current from the Monte Carlo simulation is the same as that from the common formalism for a certain value of ψ (the master angle); the value of the master angle was smaller than 54.7° and depended on the exit angle and subshell.

ACKNOWLEDGMENT

One of the authors (A.J.) would like to acknowledge the support of Grant No. KBN 2 2466 91 02.

-
- ¹O. A. Baschenko and V. I. Nefedov, *J. Electron Spectrosc. Relat. Phenom.* **17**, 405 (1979); **21**, 153 (1980); **27**, 109 (1982).
- ²O. A. Baschenko, G. V. Machavariani, and V. I. Nefedov, *J. Electron Spectrosc. Relat. Phenom.* **34**, 305 (1984).
- ³A. Jablonski, *Surf. Interf. Anal.* **14**, 659 (1989).
- ⁴A. Jablonski and S. Tougaard, *J. Vac. Sci. Technol. A* **8**, 106 (1990).
- ⁵W. H. Gries and W. Werner, *Surf. Interf. Anal.* **16**, 149 (1990).
- ⁶W. S. M. Werner, *Surf. Sci.* **251/252**, 336 (1991); *Appl. Surf. Sci.* **70/71**, 29 (1993).
- ⁷V. M. Dwyer, *Surf. Interf. Anal.* **20**, 687 (1993).
- ⁸A. Jablonski and J. Zemek, *Phys. Rev. B* **48**, 4799 (1993).
- ⁹A. Jablonski and C. J. Powell, *Surf. Interf. Anal.* **20**, 771 (1993).
- ¹⁰C. J. Powell, A. Jablonski, S. Tanuma, and D. R. Penn, *J. Electron Spectrosc. Relat. Phenom.* **68**, 605 (1994).
- ¹¹A. Jablonski, *Phys. Rev. B* **43**, 7546 (1991).
- ¹²A. Jablonski, C. Jansson, and S. Tougaard, *Phys. Rev. B* **47**, 7420 (1993).
- ¹³R. A. Bonham and T. G. Strand, *J. Chem. Phys.* **39**, 2200 (1963).
- ¹⁴S. Tanuma, C. J. Powell, and D. R. Penn, *Surf. Interf. Anal.* **11**, 577 (1988); **17**, 911 (1991).
- ¹⁵I. M. Band, Yu. I. Kharitonov, and M. B. Trzhaskovskaya, *At. Data Nucl. Data Tables* **23**, 443 (1979).
- ¹⁶R. F. Reilman, A. Msezane, and S. T. Manson, *J. Electron Spectrosc. Relat. Phenom.* **8**, 389 (1976).
- ¹⁷J.-T. J. Huang, J. W. Rabalais, and F. O. Ellison, *J. Electron Spectrosc. Relat. Phenom.* **6**, 85 (1975).
- ¹⁸T. A. Carlson, *Surf. Interf. Anal.* **4**, 125 (1982).
- ¹⁹J. A. R. Samson, *J. Opt. Soc. Am.* **59**, 356 (1969).
- ²⁰J. Zemek and A. Jablonski, in *Proceedings of the 4th International Symposium on Surface Physics*, edited by J. Koukal (Elsevier, Amsterdam, 1988), p. 357.
- ²¹R. Shimizu and Z.-J. Ding, *Rep. Prog. Phys.* **55**, 487 (1992).
- ²²C. J. Powell and P. E. Larson, *Appl. Surf. Sci.* **1**, 186 (1978).
- ²³M. P. Seah, *Surf. Interf. Anal.* **2**, 222 (1980); **9**, 85 (1986).
- ²⁴M. F. Ebel, H. Ebel, and K. Hirokawa, *Spectrochim. Acta B*

- 37, 461 (1982).
- ²⁵W. Hanke, H. Ebel, M. F. Ebel, A. Jablonski, and K. Hirokawa, J. Electron Spectrosc. Relat. Phenom. **40**, 241 (1986).
- ²⁶J. E. Fulghum, Surf. Interf. Anal. **20**, 161 (1993), and references therein.
- ²⁷W. S. M. Werner, G. C. Smith, and A. K. Livesy, Surf. Interf. Anal. **21**, 38 (1994).
- ²⁸W. S. M. Werner, Surf. Interf. Anal. **18**, 217 (1992).